

EXPERIMENTAL INVESTIGATION OF THE EMBEDDED MICRO-CHANNEL MANIFOLD COOLING FOR POWER CHIPS

by

**Nan ZHANG^{a,b}, Ruiwen LIU^b, Yanmei KONG^b, Yuxin YE^b,
Xiangbin DU^b, Bo CONG^b, Lihang YU^b, Zhiqiang WANG^c, Yang DAI^c,
Wei LI^c, Binbin JIAO^{b*}, and Zhiyong DUAN^{a*}**

^a School of Physics and Microelectronics, Zhengzhou University, Zhengzhou, China

^b Institute of Microelectronics of the Chinese Academy of Science, Beijing, China

^c Information Science Academy of China Electronics Technology Group Corporation, Beijing, China

Original scientific paper

<https://doi.org/10.2298/TSCI210908328Z>

Power chips with high power dissipation and high heat flux have caused serious thermal management problems. Traditional indirect cooling technologies could not satisfy the increasing heat dissipation requirements. The embedded cooling directly inside the chip is the hot spot of the current research, which bears greater cooling potential comparatively, due to the shortened heat transfer path and decreased thermal resistance. In this study, the thermal behaviors of the power chips were demonstrated using a thermal test chip, which was etched with micro-channels on its substrate's backside and bonded with a manifold which also fabricated with silicon wafer. The chip has normal thermal test function and embedded cooling function at the same time, and its size is $7 \times 7 \times 1.125 \text{ mm}^3$. This paper mainly discussed the influence of width of micro-channels and the number of manifold channels on the thermal and hydraulic performance of the embedded cooling structure in the single-phase regime. Compared with the conventional straight micro-channel structure, the cooling coefficient of performance of the 8×-50 (number of manifold distribution channels: 8, micro-channel width: $50 \mu\text{m}$) structure is 3.38 times higher. It is verified that the 8×-50 structure is capable of removing power dissipation of 300 W (heat flux: 1200 W/cm^2) at a maximum junction temperature of 69.6°C with pressure drop of less than 90.8 kPa. This study is beneficial to promote the embedded cooling research, which could enable the further release of the power chips performance limited by the dissipated heat.

Key words: *embedded cooling, manifold, micro-channel, thermal test chip, power chip*

Introduction

The smaller size and higher integration level of power chips has led to the increase of power dissipation, accompanied with a sharp promotion of the heat flux density, surpassing 1000 W/cm^2 [1, 2], which poses tough challenges to the thermal management. Until now, the indirect liquid cooling method, which utilizes a separated heat sink bonded with the silicon die by a thermal interface material (TIM) [3], has been used as a traditional method to address the thermal problem [4-6]. But, in this remote cooling method, the efficiency of heat transfer

* Corresponding author's, e-mail: jiaobinb@ime.ac.cn, duanzhiyong@zzu.edu.cn

is severely constrained due to the parasitic thermal interface layers and spreading resistances between the power chip and attached heat sink. Studies have shown that the thermal resistance of the integration- introduced TIM layer accounts for 70% of the total thermal resistance on the heat transfer path [7]. The embedded cooling (intra-chip cooling) method is a transformative high-efficiency heat dissipation scheme. The cooling structure is directly deployed on the substrate of the chip, and the coolant fluid can permeate into the interior of the chip for efficient heat exchange, which provides eight times reduction in system-level thermal resistance than indirect cooling [8].

Tuckerman [9] firstly proposed a micro-channel heat sink with parallel micro-channels etched in the silicon substrate for cooling electronics in the 1980's. The single-phase water as the coolant fluid was used to dissipate 800 W/cm^2 at 186 kPa, and the total thermal resistance is $0.1 \text{ cm}^2\text{K/W}$. Since then, the embedded micro-channel cooling methods have been widely studied for high-power electronics thermal management [10-17]. It can remove higher heat flux due to its large contact area with working fluid and lower thermal resistance. However, it might result in a higher pressure drop and a large surface temperature gradient, due to the long flow path of the coolant fluid along the length of micro-channels. An attractive method is the use of a manifold structure to distribute coolant fluid through embedded heat transfer structure, which can improve the temperature uniformity and increase the cooling efficiency without increasing pressure drop compared to conventional micro-channel cooling [18-20].

Kong *et al.* [13] experimentally studied the single-phase thermal and hydraulic performance of embedded micro pin-fin arrays using a titanium-gold layer as the heaters, and achieved a maximum heat transfer coefficient of $18.2 \text{ kW/m}^2\text{K}$ at a pressure drop of 47 kPa. Jung *et al.* [21] experimentally studied the cooling performance of an 3-D manifold micro-channel heat sink. The titanium-gold layer was deposited on the top surface of the silicon as the heaters. The heat flux of 250 W/cm^2 was effectively removed at a maximum surface temperature of $90 \text{ }^\circ\text{C}$ and a pressure drop of 3 kPa. Drummond *et al.* [22] demonstrated a hierarchical manifold micro-channel heat sink array. The titanium-gold layer as the heat source, the reported maximum heat flux up to 910 W/cm^2 was removed with less than 162 kPa using HFE-7100 as the two-phase coolant fluid. In most literatures, researchers used the metal film layer as the heaters. The heat distributes in the plane above of the substrate initially during these aforementioned heating methods, which cannot perfectly characterize the interior thermal behavior of the power chips.

In this paper, a thermal test chip (TTC) was used to emulate the thermal behaviors of the power chips, the chip with functions of microfluidics and electronics was realized through the integration of the silicon manifold and the TTC. The influence of the width of the micro-channel and number of the manifold distribution channels on the thermal and hydraulic performance was experimentally discussed. Moreover, the cooling efficiency of embedded manifold micro-channel structure was compared with a conventional straight micro-channel structure.

Test module design and fabrication

Design and fabrication of chip with embedded cooling structure

Figure 1(a) describes the conceptual design and working principle of the power chips with embedded cooling structure. Power chip embedded the heat transfer structure is in-

tegrated to the manifold. The coolant flows into the manifold system by multiple coolant inlet located in the bottom of the manifold, and the coolant is branched into two streams in opposite directions, fig. 1(c). As the coolant uniformly flows along the tapered distribution channels, the coolant impinges on the base of the embedded micro-channel. After effective heat exchange with the fins of the embedded micro-channels, the coolant then undergoes a 180° turn and merges into the tapered collection channels, which guided to the coolant exit the chip through coolant outlet located on both sides of the manifold, fig. 1(b).

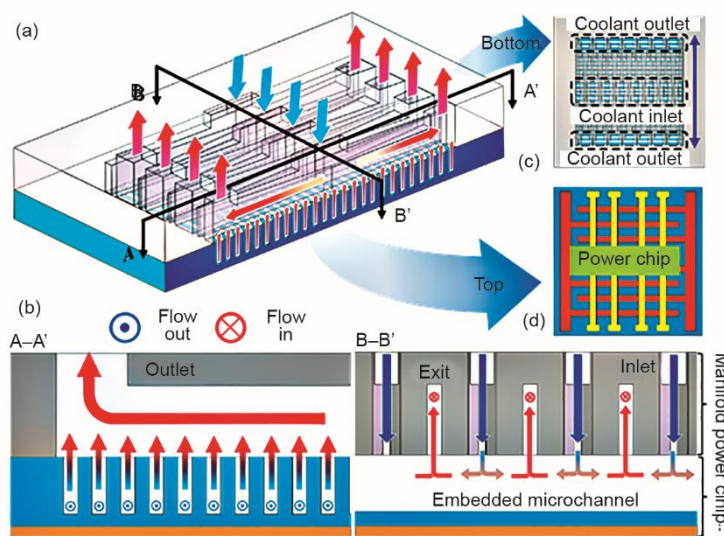


Figure 1. Conceptual design of a power chip with embedded cooling structure

In order to verify this embedded cooling method has good cooling performance for power chips. The TTC integrated heaters and temperature sensitive diodes (TSD) was fabricated on an 8-inch silicon wafer by standard COMS processing technology. A 7 mm × 7 mm TTC consists the 5 × 5 array heater cells covering a 25 mm² heating area, and each heater cell integrated a TSD in the center. In all experiments, the thermal performance of the TTC is characterized by measuring the temperature of nine heating cells is shown in fig. 2(a). The width of micro-channel and the number of manifold distribution channels combine to determine the cooling performance of the embedded cooling structure. Using deep reactive ion etching technology, a series of 300 μm, depth embedded micro-channels with widths of 150 μm, 100 μm, and 50 μm were etched on the back side of substrate. The manifold with 4, 6, and 8 distribution channels were etched on a 725 μm thick silicon wafer, referred to as the 4×, 6×, and 8× manifold. It should be noted that the coolant distribution channels and the collection channels of the three kinds of manifolds have the same dimensions. After then, the coolant inlet and outlet holes at the corresponding positions of the manifold was etched using laser etching technology.

Figure 2(a) shows the dimensions of the embedded micro-channel and the cooling area, the crucial dimensions of each feature in the manifold is shown in fig. 2(b). Table 1 lists the defined structural dimensions, as well as photographs of the manifolds and SEM images of the embedded micro-channels. After the micro-structures of the manifold and embedded micro-channel were defined, the manifold and TTC was cleaned in a Piranha bath to remove

residual organic polymer on the surface. To form the interfacial bonding layers, the 30 nm thick graphene and 200 nm gold was deposited on bottom surface of the TTC and top surface of the manifold by magnetron sputtering process. Then, the manifold and TTC were bonding at a high temperature of 420 °C and a high pressure of 450 kPa, fig. 2(b).

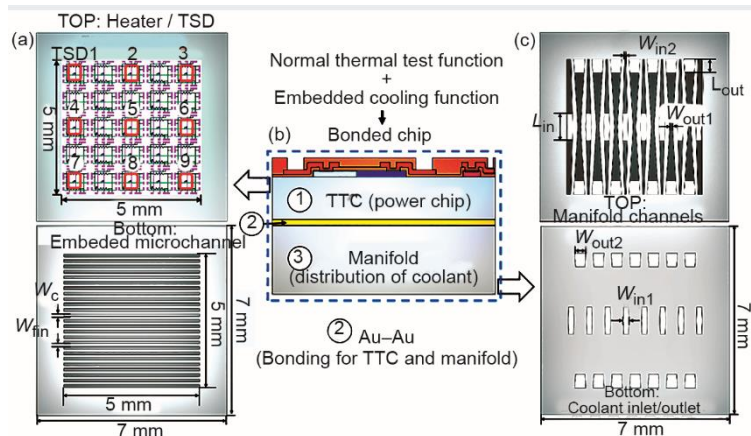

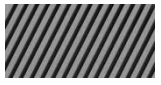

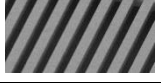

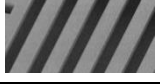


Figure 2. The relevant dimensions of each part in the TTC with embedded cooling structure

Table 1. Dimensions of structures in the embedded micro-channels and the manifold

Manifold				Embedded micro-channel			
Samples		Symbols	Dimensions	Samples		Symbols	Dimensions
4×		W_{in1}	0.2 mm	50		W_c	50 mm
		W_{in2}	0.05 mm			W_{fin}	50 mm
6×		L_{in}	1 mm	100		W_c	100 mm
		W_{out1}	0.1 mm			W_{fin}	100 mm
8×		W_{out2}	0.4 mm	150		W_c	150 mm
		L_{out}	0.5 mm			W_{fin}	150 mm

Test module assembly

As shown in fig. 3(b), a 2.5 mm thick printed circuit board (PCB) was designed to provide electrical/fluidic interfaces for the chip, the coolant inlet and outlet openings on the chip and the PCB mate with each other. The bonding ring was fabricated in the middle of the PCB, the chip was bonded to the top side of PCB using solder paste. In addition, the heaters and TSD were, respectively, wire bonded to the power pads and TSD pads on the top surface of PCB through a set of gold wires. An 8 mm thick polymethyl methacrylate layer (PMMA) serves as an interface between the chip and the flow loop and contains the threaded holes for the test module assembly. The coolant inlet and outlet were located on the side of the manifold base. For assembly of the test module, a 1 mm thick silicone gasket was laser-cut to realize the circulation of coolant, which was sandwiched between the PCB and PMMA to prevent the leakage of coolant during the experiment. Figure 3(a) shows the photograph of the assembled

test module, the quick connectors were installed on the PMMA for circulation of coolant in the flow loop and connection differential manometer and thermocouples. The heaters of TTC were all wired in parallel to a power supply (IT6522D, ITECH), the TSD were respectively connected to the standard temperature signal acquisition module (STSA-M) during the test.

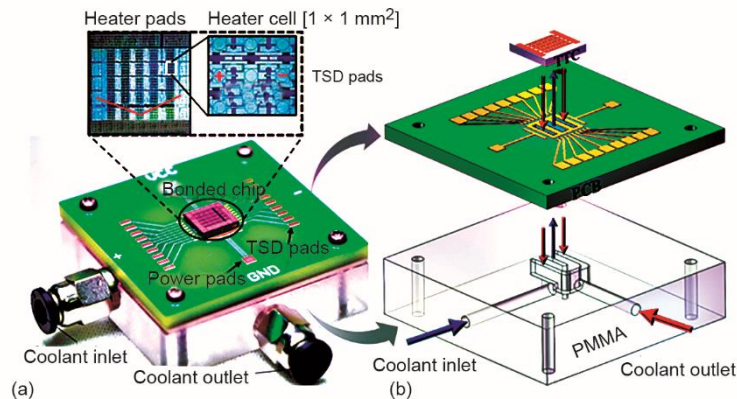


Figure 3. Assembly of the test module; (a) an image of the assembled test module and (b) design details of the test module

Experiment methods

Flow loop

A closed flow loop is shown schematically in fig. 4. The deionized water was used as the coolant fluid. When the test module was installed into the closed flow loop, the coolant was pumped from a large volume reservoir to the test module and back by an infusion pump (Y-600, XYHY). The pressure drop across the test module was measured using a differential manometer (DPG409-050DWU, OMEGA). The coolant temperature was measured by the *T*-type thermocouples inserted into the test module inlet and outlet. After the coolant flowed

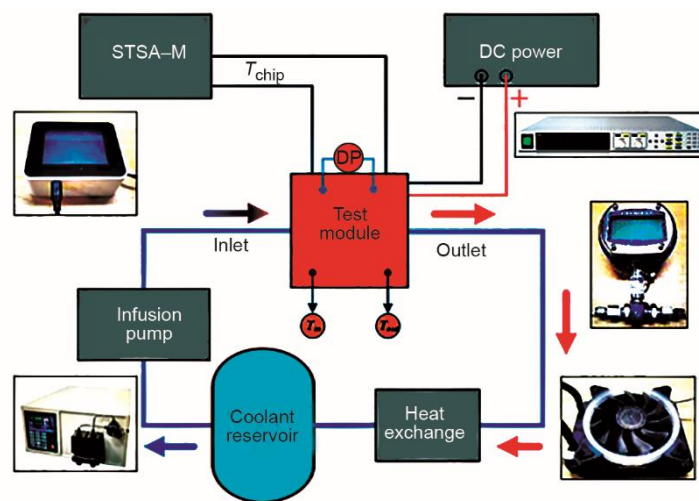


Figure 4. Schematic diagram of the closed flow loop

through the test module, an air-cooled heat exchanger was used to removal the heat from the heated coolant and control the coolant temperature at the room conditions before returning to the reservoir.

Data reduction

Electrical power supplied to the TTC, Q_{ttc} , is calculated by multiplying the supplied voltage and current in the power supply. The net heat input transferred to the coolant, Q_{heater} , is estimated by the measuring the sensible heat change of the coolant fluid:

$$Q_{\text{heater}} = \dot{m} \int_{T_{\text{in}}}^{T_{\text{out}}} C_p(T) dT \quad (1)$$

where C_p is the saturated specific heat of the single-phase deionized water, T_{in} – the coolant inlet temperature, which is the room temperature of 25.2 °C, and T_{out} – the coolant temperature flowing after the TTC. Nine TSD distributed on the surface of the TTC, fig. 2(a), are used to characterize the thermal performance, the cooling uniformity is evaluated by the standard deviation of the temperature (SDT), and the TTC maximum temperature, $T_{\text{tcc,max}}$, is calculated by taking the maximum temperature of the TSD1-9:

$$\text{SDT} = \sqrt{\frac{1}{n} \sum_{i=1}^n (T_i - T')^2} \quad (2)$$

where n is the number of the working TSD in this experiment and T' – the average temperature of the TSD1-9.

The total thermal resistance, R_{total} , consists of conduction, $R_{\text{conduction}}$, convection, $R_{\text{convection}}$, and advection, $R_{\text{advection}}$, thermal resistances:

$$R_{\text{total}} = \frac{(T_{\text{tcc,max}} - T_{\text{in}}) A_{\text{heater}}}{Q_{\text{heater}}} \quad (3)$$

$$R_{\text{advection}} = \frac{(T_{\text{out}} - T_{\text{in}}) A_{\text{heater}}}{Q_{\text{heater}}} \quad (4)$$

$$R_{\text{conduction}} = \frac{(T_{\text{tcc,base}} - T_{\text{in}}) A_{\text{heater}}}{Q_{\text{heater}}} \quad (5)$$

$$R_{\text{total}} = R_{\text{convection}} - R_{\text{advection}} - R_{\text{conduction}} \quad (6)$$

where A_{heater} is the heated area of the TTC.

The heat transfer coefficient, h_{wall} , is defined as a convective heat transfer rate inside the embedded micro-channel walls:

$$h_{\text{wall}} = \frac{Q_{\text{heater}}}{A_{\text{wet}} (T_{\text{tcc,base}} - T_{\text{in}}) \eta_0} \quad (7)$$

where A_{wet} is the micro-channel wetted area and η_0 – the overall fin efficiency.

The $T_{\text{ttc,base}}$ is the average temperature of the embedded micro-channel base, which is estimated by accounting the conduction resistances between the heater and micro-channel base:

$$T_{\text{ttc,base}} = T_{\text{ttc,max}} - \frac{Q_{\text{heater}}}{A_{\text{heater}}} \left(\frac{d_{\text{SiO}_2}}{k_{\text{SiO}_2}} + \frac{d_{\text{Si}}}{k_{\text{Si}}} \right) \quad (8)$$

$$\eta_0 = 1 - \frac{N_{ec} A_{\text{fin}}}{A_{\text{wet}}} (1 - \eta_{\text{fin}}) \quad (9)$$

where N_{ec} is the number of the micro-channels, A_{fin} – the micro-channel fins area, η_{fin} – the fin efficiency, d_{Si} – the thickness of the substrate, and d_{SiO_2} – the thickness of the insulation layer.

$$\eta_{\text{fin}} = \frac{\tanh \left(H_c \sqrt{\frac{2h_{\text{wall}}}{k_{\text{Si}} W_{\text{fin}}}} \right)}{H_c \sqrt{\frac{2h_{\text{wall}}}{k_{\text{Si}} W_{\text{fin}}}}} \quad (10)$$

where H_c represents the micro-channel depth, W_{fin} – the micro-channel wall width, and k_{Si} – the substrate thermal conductivity. The h_{wall} is determined assuming $\eta_{\text{fin}} = 1$ as a starting point until the calculated value, h_{wall} , was converged. The energy efficiency of the cooling structure is evaluated by the cooling COP, which is defined as the ration of removing power to the pumping power at a given maximum chip temperature. The P_{pump} is calculated as the product of the coolant flow rate and system pressure drop:

$$\text{COP} = \frac{Q_{\text{heater}}}{P_{\text{pump}}} \quad (11)$$

Uncertainty

In this experiment, the working range and measurement accuracy of the experimental tools are listed in tab. 2. The TSD were used to measure the surface temperature of TTC. Before testing, the TTC was placed in an oven (ESPEC, SH-242) and calibrated at different temperature points. The accuracy of the TSD is calculated by the accuracy of the oven and the repeatability of the TSD over time. The accuracy of the other tools was obtained from the user manual of the products.

Table 2. A list of experimental tools and their accuracy information

Parameter	Experimental	Range	Accuracy
Coolant temperature [°C]	Thermocouple	–50-200	±1 °C
Volumetric flow rate [mL per minute]	Infusion pump	0-1000	±0.5%
Pressure drops [kPa]	Differential manometer	0-350	±0.1%
TTC temperature [°C]	TSD (calibrated)	–20-250	±0.5 °C
Power [W]	Power supply	0-3000	0.05% + 30 mV, 0.2% + 120 mA

Result and discussion

The influence of embedded cooling structure designs on thermal and hydraulic performance

The width of micro-channel and the number of manifold distribution channels is an important factor to influence the thermal and hydraulic performance of the TTC with embedded cooling structure. To evaluate the performance of different cooling structure designs according to their total thermal resistance, wall heat transfer coefficient, cooling uniformity, and system pressure drop as the flow rate increases from 200 mL per minute to 400 mL per minute for a given heat flux of 1200 W/cm^2 . This experiment set up five cooling structures of 4×-50 , 6×-50 , 8×-50 , 8×-100 , and 8×-150 (manifold distribution channels number \times micro-channel width, tab. 1) in these experiments.

Figure 5(a) shows the total thermal resistance of five embedded cooling structures as a function of the flow rate. It is obvious that the total thermal resistance decreases as the flow rate increases. For a fixed micro-channels width (50 μm), the 6×-50 structure provided the lowest total thermal resistance and the 4×-50 structure provided the highest, but this difference between each other is no significant. The increase in the number of manifold distribution channels results in a more uniform local coolant flow through the embedded heat transfer structure. Therefore, the total thermal resistance decreases as the number of manifold distribu-

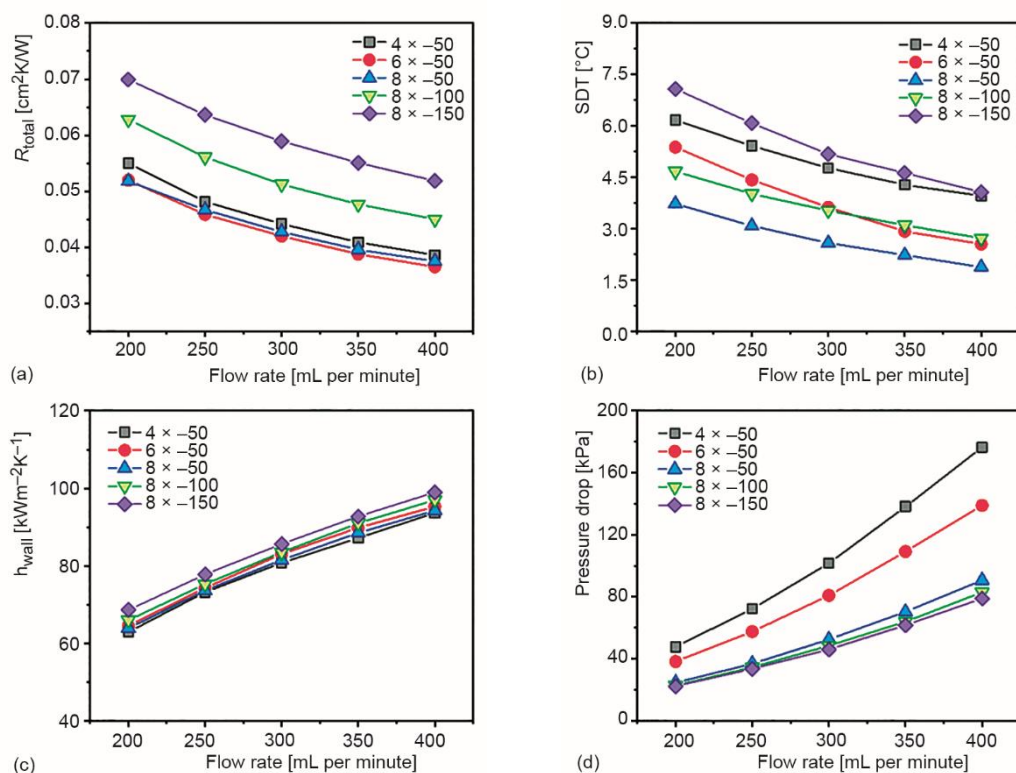


Figure 5. Thermal and hydraulic performance comparison of different embedded cooling structures under the same heat flux of 1200 W/cm^2 ; (a) total thermal resistance, (b) cooling uniformity, (c) wall heat transfer coefficient, and (d) system pressure drop

tion channels increases from 4-6, the coolant flow path through the embedded micro-channels is reduced, and increased the jet impact effect on the micro-channels base. However, the total thermal resistance increases as the number of manifold distribution channels further increases to 8. This phenomenon is due to reduction in the local flow rate through one unit cell of the heat transfer structure, which causes the deterioration of cooling performance [23]. For a fixed $8 \times$ manifold structure, the 8×-50 structure has the lowest thermal resistance and the 8×-150 structure has the highest thermal resistance, which can be attributed to the increases of the wetted area for heat transfer as the width of micro-channels decreases from $150 \mu\text{m}$ to $50 \mu\text{m}$.

The cooling uniformity of the embedded cooling structures is characterized by the SDT, as shown in fig. 5(b). The number of manifold channels has significant influence on the cooling uniformity. Under the same conditions, the cooling uniformity could be improved by increasing the manifold distribution channels which results in a more uniform coolant fluid distribution along the micro-channel, and it could also be improved with the decreases of the micro-channel width as the coolant distribution along the manifold distribution is more uniform. For the 8×-50 structure, the SDT is 1.88°C at the flow rate of 400 mL per minute.

The heat transfer coefficient as a function of flow rate is plotted in fig. 5(c). In general, the convective heat transfer rate at the wall of the embedded micro-channels increases with the flow rate. The 6×-50 structure has a higher heat transfer coefficient compared to 4×-50 and 8×-50 structures due to the effective and uniform heat transfer of the coolant fluid inside the micro-channels. However, this difference between each other is no significant. For a fixed $8 \times$ manifold, the embedded cooling structure with wider micro-channels has a larger heat transfer coefficient than cooling structure with thinner micro-channels, this is due to the reduced flow resistance in the wider micro-channels, thus allowing for better coolant fluid replenishment at the lower portions of the micro-channels (near the embedded micro-channels base) [22].

The system pressure drops verses flow rate is shown in fig. 5(d). In the signal-phase regime, the system pressure drop remains relatively constant with increasing heat flux. The system pressure drop across the test module consist the pressure losses caused by the contraction into resistance and expansion out resistance of the embedded micro-channels, that of the coolant splitting and expansion/contraction resistance of the manifold channels. At a constant $50 \mu\text{m}$ width micro-channel, the 8×-50 structure exhibits the smallest pressure drop under the same conditions, which reduces the coolant flow path through the embedded micro-channels. It is noted that the rate of increase in pressure drop slows down as the number of manifold channels increases, the pressure drop caused in the manifold channels will increase with the flow rate through one distribution channel of manifold increases at the same volumetric flow rate conditions. For a fixed $8 \times$ manifold, since the flow resistance of the embedded heat exchange structure increases as the width of micro-channels decreases from $150 \mu\text{m}$ to $50 \mu\text{m}$, the system pressure drop across the TTC slightly increases. Here, since the influence of the manifold channels on the system pressure drop is dominant, the change in the width of the micro-channels has a small effect on the system pressure drop.

Cooling performance of the TTC with 8×-50 cooling structure

In order to evaluate the thermal performance of TTC with embedded cooling structure at different heat flux conditions, the maximum temperature of the TTC, $T_{\text{tc,max}}$, heat transfer coefficient, h_{wall} , and the total thermal resistance, R_{total} , were measured and analyzed with 8×-50 structure.

Figure 6(a) shows the maximum temperature of the TTC vs. heat flux at five volumetric flow rates. The maximum temperature for any given flow rate is increased linearly as

the heat flux increases, this is due to the supplied heat flux is less than the value required to reach the saturation temperature, the coolant fluid therefore remains in a single-phase regime. At a constant heat flux, the maximum temperature is reduced with increase flow rate. The maximum heat flux of 1200 W/cm^2 is removed at the flow rate of 400 mL per minute and the maximum temperature is 69°C .

Figure 6(b) shows the wall heat transfer coefficient vs. flow rate for given heat flux. In the single-phase regime, the thickness of the thermal boundary layer decreases as the flow rate increases [23]. Therefore, the heat transfer coefficient increases significantly as the flow rate increases. The heat transfer coefficient also shows a weaker dependence on heat flux, which increases with the heat flux due to increase in thermal conductivity of the coolant. Thus, it is effective to improve the heat transfer coefficient though increasing the flow rate.

Figure 6(c) shows the total thermal resistance as a function of flow rate. For a given heat flux, the total thermal resistance decreases significantly as the flow rate increases, which is due to reduction of the advection and convection thermal resistance with increasing flow rate, as shown in fig. 5(d). At the heat flux of 1200 W/cm^2 , when the coolant flow rate is increased from 200-400 mL per minute, the proportion of advection thermal resistance in total thermal resistance is reduced from 32.6% to 22.4%, and the convection and conduction thermal resistance in total thermal resistance is on the rise. In addition, the convection and advection thermal resistances represents about 78.9% of the total thermal resistance at the flow rate

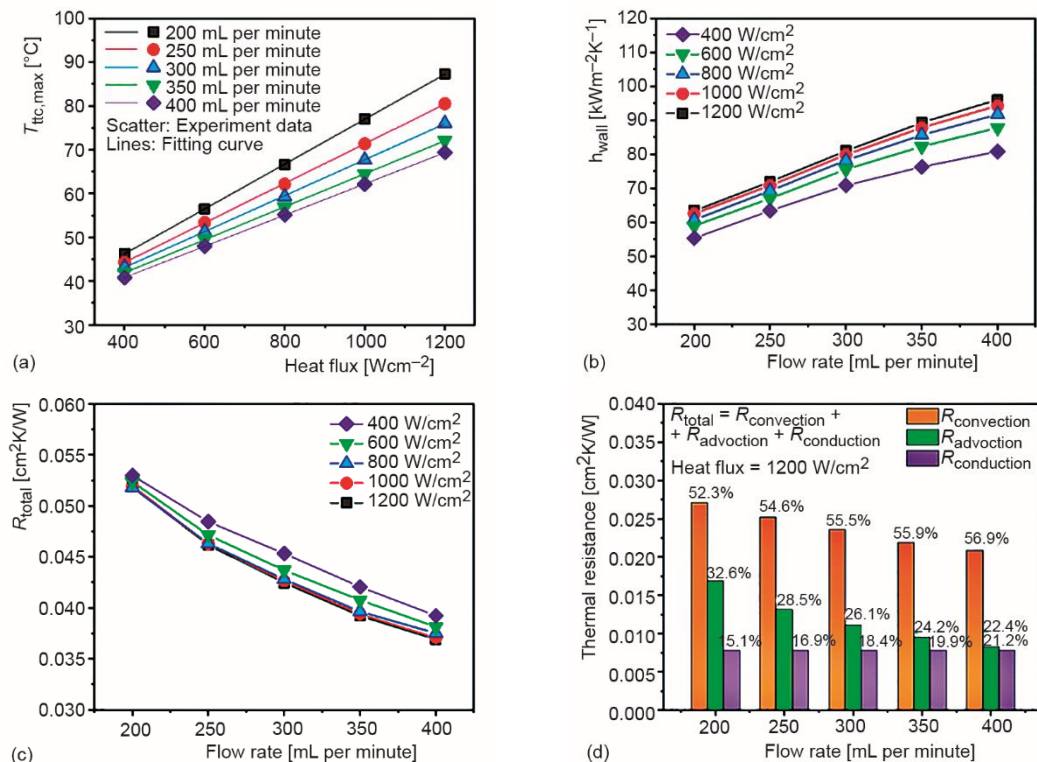


Figure 6. The cooling performance of the TTC with embedded 8×-50 cooling structure; (a) maximum temperature, (b) wall heat transfer coefficient, (c) total thermal resistance, and (d) composition of each thermal resistance component

of 400 mL per minute, see fig. 6(d). There is room for further reducing the total thermal resistance by increasing the coolant flow rate.

Cooling efficiency comparison of embedded manifold micro-channel structure and conventional straight micro-channel structure

In order to evaluate the effectiveness of the embedded manifold micro-channel structure, here the cooling efficiency of a straight micro-channels structure with the same width 50 μm was compared with it. As shown in fig. 7(a), the energy efficiency of cooling system is evaluated by the cooling COP, which was calculated using eq. (11) for a maximum temperature rise of 60 $^{\circ}\text{C}$ at a constant heat flux of 1200 W/cm^2 . The energy efficiency improves with increasing number of manifold distribution channels and decreasing the width of micro-channels. The 8×-50 structure has the largest COP at all the samples, which can obtain approximately 3.38 times higher COP than 50 μm straight micro-channels. The measured pumping power vs. flow rate for the conventional straight micro-channels structure and embedded micro-channel manifold structure is shown in fig. 7(b). The maximum pumping power of the 50 μm straight micro-channels is 1.05 W at the flow rate of 400 mL per minute. For the 8×-50 structure, a maximum pumping power of 0.6 W was calculated at a 400 mL per minute flow rate. It is observed that under an equivalent pumping power (e.g. 0.6 W, as highlighted by a gray dashed line) the coolant flow rate through the embedded micro-channel manifold structure is approximately 1.3 times higher than straight micro-channels structure. Conversely, it can be deduced from the pumping power vs. flow rate curve that, with the increase of flow rate, the pumping power difference between the straight micro-channels structure and the embedded micro-channel manifold structure will be significantly get bigger.

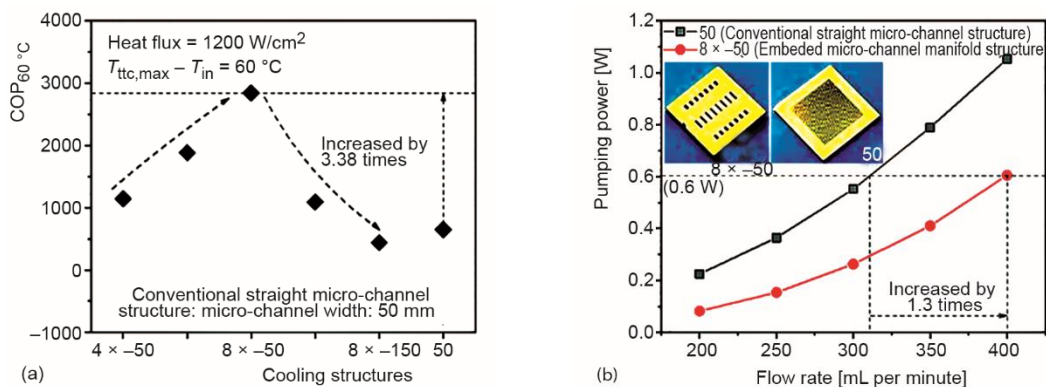


Figure 7. The cooling efficiency comparison of embedded micro-channel manifold structure with conventional straight micro-channels structure; (a) COP comparison at a heat flux of 1200 W/cm^2 and (b) pumping power comparison between 8×-50 structure and 50 μm width straight micro-channel structure

Conclusions

In this work, a TTC was used to characterize the thermal behaviors of the power chips. The embedded micro-channel was etched on the back side of the TTC's substrate, and a

manifold chip was fabricated by silicon too, then two chips are bonded together to form an embedded micro-channel manifold cooling chip.

The number of manifold distribution channels and width of embedded micro-channel of the embedded cooling structures on the thermal and hydraulic performance was discussed. The results show that the cooling performance of the embedded cooling structure could be optimized by the compromise between the width of micro-channel and the number of manifold channels. For a fixed width of micro-channel, increasing the number of manifold distribution channels from 4-8 could greatly improve the cooling uniformity and reduce the pumping power. However, there is a slight limit to the optimization of the thermal resistance and heat transfer coefficient. For a fixed manifold structure, the reduction of the width of the micro-channel could effectively reduce the total thermal resistance and improve the cooling uniformity. In a thinner micro-channels, a larger system pressure drop is caused with decreasing hydraulic diameter, and the convection heat transfer efficiency is reduced due to a lower fin efficiency. The cooling structures with thinner micro-channels and more manifold channels has a better energy efficiency. The 8×-50 structure provides the best energy efficient (COP = 2846), which is 3.38 times higher than the conventional straight micro-channel structure. In single-phase regime, the embedded micro-channel manifold structure still maintains excellent cooling performance at high heat flux. The cooling method can provide highly efficient heat dissipation performance for power chips, while enabling the further release of the power chips performance limited by the dissipated heat.

Acknowledgment

This work supplied by National Key Research and Development Program (2018YFB2002902).

Nomenclature

A_{fin} – micro-channel fin area, [cm²]
 A_{heater} – heated area, [cm²]
 A_{wet} – wetted heat transfer area, [cm²]
 C_p – specific heat, [Jkg⁻¹K⁻¹]
 d – thickness, [mm]
 H – height, [mm]
 h – heat transfer coefficient, [kWm²K]
 k – thermal conductivity, [Wm⁻¹K⁻¹]
 L – length, [mm]
 \dot{m} – mass-flow rate, [kgs⁻¹]
 p – pressure drop, [kPa]
 Q – thermal power, [W]
 R – thermal resistance, [cm²KW⁻¹]

T – temperature, [°C]
 W – width, [mm]

Greek symbols

η_{fin} – individual fin efficiency
 η_0 – overall fin efficiency

Subscripts

c – embedded micro-channel
 fin – micro-channel wall
 in – inlet
 out – outlet
 max – maximum

References

- [1] Avram, B. C., et al., Gen3 Embedded Cooling for High Power RF Components, *Proceedings, IEEE International Conference on Microwaves, Antennas, Communications and Electronic Systems (COM-CAS)*, Tel-Aviv, Izrael, 2017, pp. 1-8
- [2] Avram, B. C., et al., DARPA's Intra/Interchip Enhanced Cooling (ICECool) Program, *Proceedings, Compound Semiconductor Manufacturing Technology Conference (CS MANTECH)*, New Orleans, La., USA, 2013, pp. 171-174
- [3] Li, M., et al., Synergistic Effect of Carbon Fiber and Graphite on Reducing Thermal Resistance of Thermal Interface Materials, *Composites Science and Technology*, 212 (2021), Aug., 108883
- [4] Lin, H., et al., Comprehensive Thermal Resistance Model of Forced Air Cooling System for Multiple Power Chips, *Energy Reports*, 7 (2021), Suppl. 1, pp. S261-S267

- [5] Liang, S., et al., Structural Optimization and Numerical Thermal Analysis of Ultraviolet Light-Emitting Diodes with High-Power Multi-Chip Arrays, *Optik*, 222 (2020), Nov., p. 16533
- [6] Tan, H., et al., Temperature Uniformity in Convective Leaf Vein-Shaped Fluid Micro-channels for Phased Array Antenna Cooling, *International Journal of Thermal Sciences*, 150 (2020), Apr., p. 106224
- [7] Kang, T., et al., Enhanced Thermal Management of GaN Power Amplifier Electronics with Micro-Pin Fin Heat Sinks, *Electronics*, 9 (2020), 11, 1778
- [8] John. D., Embedded Microfluidic Cooling of High Heat Flux Electronic Components, *Proceedings*, S3-P10: Lester Eastman Conference on High Performance Devices (LEC), Bethlehem, Penn., USA, 2014, pp. 1-4
- [9] Tuckerman, D. B., Implications of High-Performance Heat Sinking for Electron Devices, *IEEE Trans. Electron Devices*, 28 (1981), 10, pp. 1230-1231
- [10] Morini, G. L., Single-Phase Convective Heat Transfer in Micro-channels: A Review of Experimental Results, *International Journal of Thermal Sciences*, 43 (2004), 7, pp. 631-651
- [11] Kandlikar, S. G., High Flux Heat Removal with Micro-channels – A Roadmap of Challenges and Opportunities, *Heat Transfer Engineering*, 26 (2005), 8, pp. 5-14
- [12] Deng, D., et al., A Review on Flow Boiling Enhancement and Fabrication of Enhanced Micro-channels Of Micro-channel Heat Sinks, *International Journal of Heat and Mass Transfer*, 175 (2021), Aug., 121332
- [13] Kong, D., et al., Single-Phase Thermal and Hydraulic Performance of Embedded Silicon Micro-Pin Fin Heat Sinks Using R245fa, *International Journal of Heat and Mass Transfer*, 141 (2019), Oct., pp. 145-155
- [14] Zeng, L., et al., Thermal and Flow Performance in Micro-channel Heat Sink with Open-Ring Pin Fins, *International Journal of Mechanical Sciences*, 200 (2021), June, 106445
- [15] Farzaneh, M., et al., Design of Bifurcating Micro-channels with/without Loops for Cooling of Square-shaped Electronic Components, *Applied Thermal Engineering*, 108 (2016), Sept., pp. 581-595
- [16] Yu, X.-F., et al., A Study on the Hydraulic and Thermal Characteristics in Fractal Tree-Like Micro-channels by Numerical and Experimental Methods, *International Journal of Heat and Mass Transfer*, 55 (2012), 25-26, pp. 7499-7507
- [17] Zhuang, D., et al., Optimization of Micro-channel Heat Sink with Rhombus Fractal-like Units for Electronic Chip Cooling, *International Journal of Refrigeration*, 116 (2020), Aug., pp. 108-118
- [18] Ryu, J. H., et al., Three-Dimensional Numerical Optimization of a Manifold Micro-channel Heat Sink, *International Journal of Heat and Mass Transfer*, 46 (2003), 9, pp. 1553-1562
- [19] Zhang, Y., et al., Effects of Channel Shape on the Cooling Performance of Hybrid Micro-Channel and Slot-Jet Module, *International Journal of Heat and Mass Transfer*, 113 (2017), Oct., pp. 295-309
- [20] Andhare, R. S., et al., Heat Transfer and Pressure Drop Characteristics of a Flat Plate Manifold Micro-channel Heat Exchanger in Counter Flow Configuration, *Applied Thermal Engineering*, 96 (2016), Mar., pp. 178-189
- [21] Jung, K. W., et al., Embedded Cooling with 3-D Manifold for Vehicle Power Electronics Application: Single-Phase Thermal-Fluid Performance, *International Journal of Heat and Mass Transfer*, 130 (2019), Mar., pp. 1108-1119
- [22] Drummond, K. P., et al., A Hierarchical Manifold Micro-channel Heat Sink Array for High-Heat-Flux Two-Phase Cooling of Electronics, *International Journal of Heat and Mass Transfer*, 117 (2018), Feb., pp. 319-330
- [23] Escher, W., et al., A Novel High Performance, Ultra Thin Heat Sink for Electronics, *International Journal of Heat and Fluid Flow*, 31 (2010), 4, pp. 586-598